Hazardous radiation protective glasses for medical and research laboratories

R. Ruamnikhom [a], R. Rajaramakrishna [b,*], W. Chaiphaksa [c], W. Cheewasukhanont [d], N. Intachai [d], S. Kothan [d,**], J. Kaewkhao [c,***]

[a] Faculty of Liberal Arts, Rajamangala University of Technology Rattanakosin, Nakhon Pathom, 73170, Thailand
[b] Siberian Federal University, Svobodny Prospect 79, 660041, Krasnoyarsk, Russia
[c] Center of Excellence in Glass Technology and Materials Science (CEGM), Nakhon Pathom Rajabhat University, Nakhon Pathom, Thailand
[d] Center of Radiation Research and Medical Imaging, Department of Radiologic Technology, Faculty of Associated Medical Sciences, Chiang Mai University, Chiang Mai, 50200, Thailand

A R T I C L E   I N F O

A B S T R A C T

In the current study, the bismuth oxide (Bi_2O_3) content was inter-substituted with gadolinium oxide (Gd_2O_3) in sodium borate glass. Glass sample density and molar volume values show a reverse trend. The optical transparent radiation shielding glasses are more commonly used materials in hospitals or any hazardous radiation working environments, the glasses used in this work are more emphasized on their superior transmittance and acceptable for shielding materials for commercial purposes. The optical band gap value was calculated using the Tauc plot and absorption fitting method. Radiation shielding parameters like mass attenuation co-efficient, effective atomic number, effective electron density, equivalent atomic number, lead equivalent thickness, half value layer, tenth value layer, Geometric-Progression fitting parameters like (b, c, a, X_K, and d), γ-ray build-up factor, and exposure build-up factor have all been evaluated. In the current work, photoluminescence studies for Gd^{3+} ions were investigated and discussed.

1. Introduction

Radiation shielding materials are used in hospitals, laboratories, nuclear power plants, and nuclear waste management facility centres due to their environmental and human safety measurements. Though concrete walls could safeguard from the radiation against gamma ray, yet they do show limitations related to close-chamber setups. To overcome such near encounter hazards with close chamber setups "Glasses" are chosen [1,2] due to their transparent behaviour and shielding ability [3–6]. Also, the radiation absorbed in the glasses or in the air can be correlated to energy absorption build-up factor (BF) [5]. The intensity of gamma-ray beam follows the Beer Lambert's law ($I = I_o e^{-\mu t}$) when passed through the material medium under certain conditions [6]. The conditions are (a) mono-chromatic ray (b) thin absorbing material, and (c) narrow beam geometry. If any, one conditions are not met then Beer Lamber's law fails to meet the criteria unless a correction factor, called as "build-up factor" (BF) is used [5,6]. Borate glasses are chosen to be

superior and one of the most common glass formers and best host to accommodate higher concentration of rare-earth content with higher phonon energy than compared to other glass formers. These glasses have unique properties such as a low melting point, high thermal stability, and good, rare earth ion solubility [7,8] which makes them perfect choice for radiation shielding host [9]. Addition of modifiers such as alkali and alkaline earth ions such as sodium oxide (Na_2O) improves [10] the optical, physical, structural, and luminescence properties of the glasses [11–13]. Addition of heavy metal oxide (HMO) such as Bi_2O_3 content [14] in the sodium borate glasses increases the mechanical [15,16] and radiation shielding capability [15–19] when introduced in it. In our previous work [4,5, 20] it was observed that addition of rare-earth ions enhances the radiation shielding property and hence in the present work it is focused to add rare-earth ions with heavy metal oxide such as Bi_2O_3. Addition of rare-earth ions such as gadolinium (Gd_2O_3) content in the glass matrix will enhances the radiation shielding ability [21] and its optical transmittance which is important property for the glasses [22,23]. The rare-earth doped glasses are most importance for the manufacturing of solid-state luminous applications [24] and shielding gamma-ray and neutron applications [25]. In the present research work, the heavy metal oxide (HMO) glasses with high transparent to visible light and able to absorb the gamma ray to protect from high energy radiation. The exposure build-up factors were computed using the Geometric Progression (G-P) fitting formula for HMO glass system. G-P fitting was computed over a wide range of energy (0.015–15 MeV) and up to 40 mfp.

2. Material synthesis

$75B_2O_3+15Na_2O + xBi_2O_3+(10-x) Gd_2O_3$ where $x = 3$, 5, and 7 mol% glasses were prepared by melt quenching technique. High purity analytical grade H_3BO_3, $NaCO_3$, Bi_2O_3, Gd_2O_3 oxides were used for to prepare the glass samples. The oxide content was fine powdered in pestle and mortar. The fine powder was then transferred to silica crucible and heat treated at $1400\,°C$ for 3 h. The melt was quenched in a preheated graphite mold later heat treated at $550\,°C$ for 3 h. The prepared glasses were cut and polished into dimension length of 1 cm × breadth of 1 cm × thickness of 0.3 cm as shown in Fig. 1. The weight of the samples recorded with the 4-digit HR-200, Diethelm limited balance, both in water and air for density measurement, was used to investigate the physical properties. The refractive index (n) was determined using an Abbe refractometer, a sodium vapor lamp as a light source, and mono bromonaphthalene ($C_{10}H_7Br$) as a contact liquid. XRD measurements were carried using Shimadzu XRD-6100 instrument. At room temperature, the optical transmission spectra of glass samples of equal thickness were recorded using a spectrophotometer (Variance, Cary 50) in the UV-VIS-NIR region at 300–800 nm. Similarly, the photoluminescence excitation spectra, and emission spectra were measured by fluorescence spectrophotometer (Agilent Technologies, Cary Eclipse) with xenon lamp as a light source.

3. XRD studies

The XRD spectra show as shown in Fig. 2 show no sharp peaks rather it shows two broad diffused humps [26] near 30° and 45° not revealing to any presence of crystallinity in the structure. The study confirms that the prepared glasses are amorphous solids.

4. Density, molar volume and refractive index

The preliminary measurements such as density and molar volume of the prepared samples are as shown in Fig. 3 and Table .1. From Fig. 3 it is observed that the inclusion of bismuth at expense of gadolinium in the glass show increase in glass density while molar volume decreases. Increase in density, decrease in molar volume suggest the glass network tends to contract/shrink. At higher concentration of bismuth (7 mol%) the volume seems to slightly increase suggesting that the network expands due to larger ionic radii (Bi^{3+}). Inter-substituting of Bi^{3+}-O^{6-} ions to that of Gd^{3+}-O^{6-} ions creates less spacing in their structure due to their lower bonding distance of Bi–O (1.934 Å [27]) to that of Gd–O (2.284 Å [28] to 2.293 Å [29]).
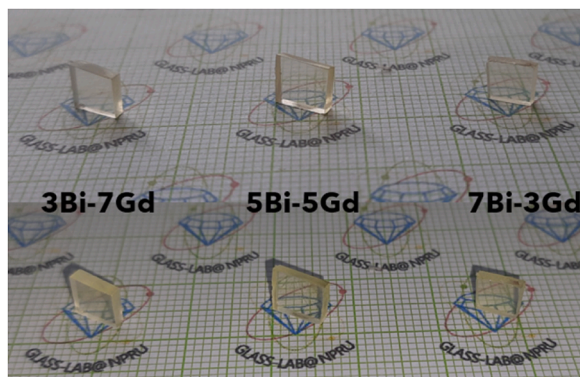

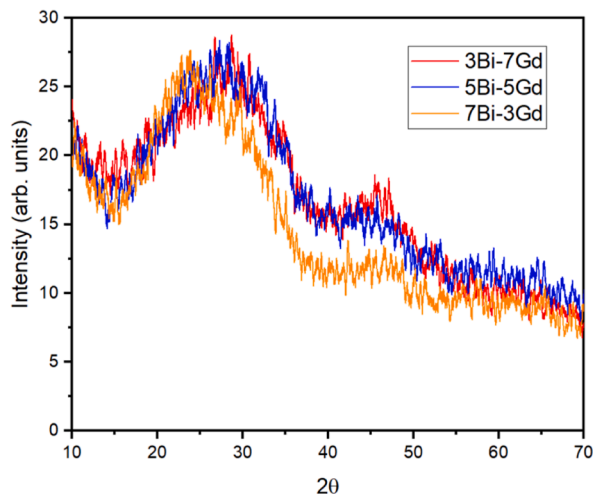**Fig. 1.** Photograph of the prepared glasses.
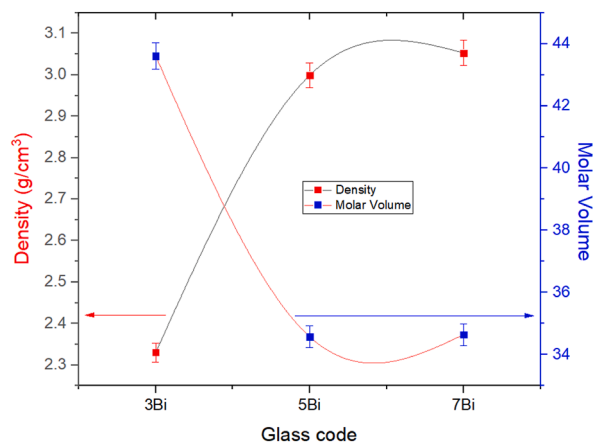
Fig. 2. XRD spectra of prepared glasses.

Fig. 3. Photograph of the prepared bismuth-gadolinium borate glasses.

Table 1
Glass composition, code, density, and molar volume of the prepared glass samples.

Glass Composition	Glass Code	Density	Molar Volume
$75B_2O_3+15Na_2O+3Bi_2O_3+7Gd_2O_3$	3Bi-7Gd	2.33026	43.610
$75B_2O_3+15Na_2O+5Bi_2O_3+5Gd_2O_3$	5Bi-5Gd	2.99920	34.573
$75B_2O_3+15Na_2O+7Bi_2O_3+3Gd_2O_3$	7Bi-3Gd	3.05269	34.645

5. Optical properties

The optical transmittance measurements were made in the range of 200–800 nm using Cary-50 UV–Vis spectrophotometer in transmittance mode. Higher transmittance (more than 75%) was observed for 3Bi-7Gd glass samples than compared to other concentrations (~72%) in the visible region as shown in Fig. 4. The energy gap evaluated using Tauc plot [30] of the prepared glass samples was analyzed as presented in Fig. 5(a) and the values are shown in Table .2. To demonstrate the absorption spectrum fitting (ASF) method [31,32] as presented in Fig. 5(b), we begin with Equation (1) and rewrite it as a function of wavelength (λ):

$$\alpha(\lambda) = B(hc)^{m-1}\lambda\left(\frac{1}{\lambda} - \frac{1}{\lambda_g}\right)^m \tag{1}$$

where λg, h, and c are wavelengths corresponding to the optical band gap, Planck's constant, and velocity of light, respectively. Using the Beer-Lambert's law, it is possible to rewrite Equation (1) as follows:
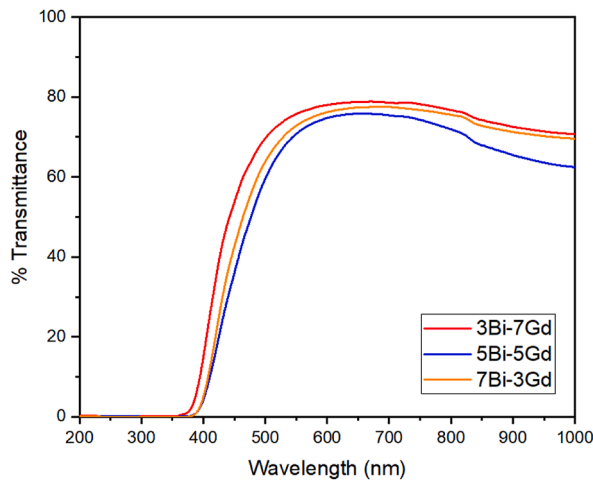
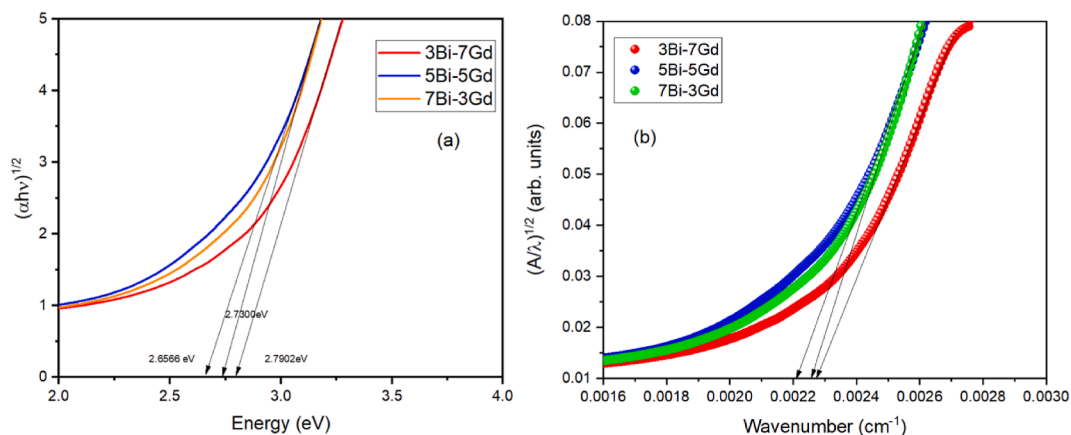**Fig. 4.** Transmittance spectra of the prepared bismuth-gadolinium borate glasses.

Fig. 5. Optical band gap spectra of the prepared bismuth-gadolinium borate glasses. (a) Tauc Plot (b) Absorption Spectrum Fitting (ASF).

Table 2
Optical thickness (d), and energy gap (eV) of the prepared glass samples.

Glass Code	Optical thickness 'd' (cm)	Optical band gap (Tauc) (eV)	Optical band gap (ASF) (eV)	Urbach Energy (E_U)
3Bi-7Gd	0.529	2.7902	2.8191	0.290
5Bi-5Gd	0.551	2.6566	2.7350	0.292
7Bi-3Gd	0.554	2.7300	2.7908	0.245

$$Abs(\lambda) = B_1\lambda\left(\frac{1}{\lambda} - \frac{1}{\lambda_g}\right)^m + B_2 \tag{2}$$

where $B_1 = [B(hc)^{m-1} \times d/2.303]$ and B_2 is a constant which consider the reflection. Using Equation (2), we can calculate the optical band gap by an absorbance spectrum fitting method without any need of glass thickness. Thus, the value of band gap, in electron volt, can be calculated from the parameter λ_g using $E_{gap}^{ASF} = 1239.83/\lambda_g$; in other words, the value of λ_g can be extrapolating the linear of the $\left(\frac{abs(\lambda)}{\lambda}\right)^{1/m}$ vs $1/\lambda$ curve at $\left(\frac{abs(\lambda)}{\lambda}\right)^{1/m} = 0$. By using least squares fit technique it was observed that the best fitting occurs for m = 2 for glasses. The values are found to be 2.819 eV, 2.7350 eV, and 2.7908 eV for 3Bi-7Gd, 5Bi-5Gd, and 7Bi-3Gd samples respectively. From Table 2 it shows the band gap values show very small deviation in their value when evaluated using Tauc plot method to that of ASF plot method this may be due to that the later method doesn't consider the thickness of the glass sample while evaluating hence we observed such difference in their value whereas they both show similar trend in these glasses. The Urbach energy has been evaluated

for the prepared glasses and shown in Fig. 6. Representing 3Bi-7Gd (Fig. 6(a)), 5Bi-5Gd (Fig. 6(b)), and 7Bi-3Gd (Fig. 6(c)). It shows that the disorderness in the glass increases with increase in Bi_2O_3 content.

6. Radiation shielding measurements

6.1. Mass attenuation coefficient (μ_m)

The mass attenuation coefficient (μm) of the glass samples is calculated by using mixture rule [33–35] as shown in Equation (3).

$$\mu_m = ln\left(\frac{I_o}{I}\right) \Big/ \rho t \tag{3}$$

where ρ is the density of glasses (g/cm³), I is the intensity of the attenuation beam, I_0 is the incident intensities and t is the thickness of glass samples (cm).

6.2. Effective atomic number and electron density

The effective atomic number and the electron density was evaluated using Equations (4) and (5) [4,5,34,35].

$$Z_{eff} = \frac{\sigma_{t,a}}{\sigma_{t,el}} \tag{4}$$

$$N_{eff} = \frac{\mu_m}{\sigma_{t,el}} \tag{5}$$

6.3. Half value layer (HVL)

Relation of HVL to linear attenuation coefficient ($\mu_L = \mu_m \times \rho$) defined by the following Equation (6) [34].
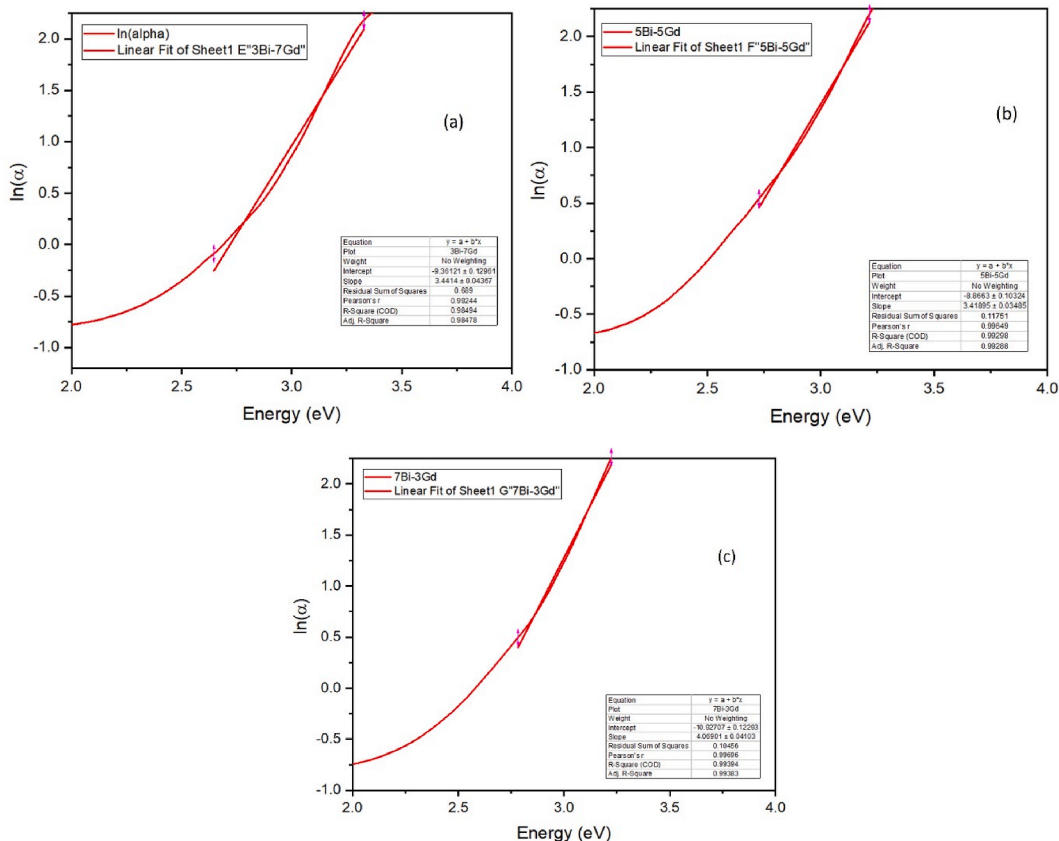

Fig. 6. Urbach Energy of the prepared bismuth-gadolinium borate glasses. (a) 3Bi-7Gd (b) 5Bi-5Gd (c) 7Bi-3Gd Glass samples.

$$x_{1/2} = \left(\frac{0.693}{\mu_L} \right) \tag{6}$$

6.4. Tenth value layer (TVL)

The relation of TVL to linear attenuation coefficient (μ) defined by following Equation (7) [34].

$$x_{1/10} = \left(\frac{2.3026}{\mu_L} \right) \tag{7}$$

6.5. Lead equivalent thickness

The lead equivalent thickness is the thickness of lead (pb) is evaluated using the relation.

$$d_{lead} = \left(\frac{\mu_{glass}}{\mu_{lead}} \right) \times d_{glass} \tag{8}$$

where d_{lead} is the lead equivalent thickness, μ_{glass} is the linear attenuation coefficient of glass samples, μ_{lead} is the linear attenuation coefficient of lead, d_{glass} is the thickness of glass samples.

6.6. Equivalent atomic number 'Z_{eq}'

Equivalent atomic number (Z_{eq}) is evaluated for the glass samples at energy range of 0.015–15 MeV using Equation (8).

$$Z_{eq} = \frac{Z_1(log\ R_2 - logR) + Z_2(logR - log\ R_1)}{log\ R_2 - log\ R_1} \tag{9}$$

where Z_1 and Z_2 are the atomic numbers corresponding to the ratio R_1 and R_2, respectively. R is the ratio of the given glasses at specific energy.

6.7. Geometric progression (G-P) fitting

Using the obtained values of 'Z_{eq}' the G-P fitting parameters such as *b, c, a, X_K,* and *d* was evaluated using Equation (9) [5,35,36].

$$P = \frac{P_1\left(log\ Z_2 - log\ Z_{eq}\right) + P_2\left(log\ Z_{eq} - log\ Z_1\right)}{log\ Z_2 - log\ Z_1} \tag{10}$$

6.8. Gamma-ray build-up factors

The values obtained from Equations (8) and (9) were used to evaluate build-up factor for the present glasses using Equations (10)–(12) [5,35,36].
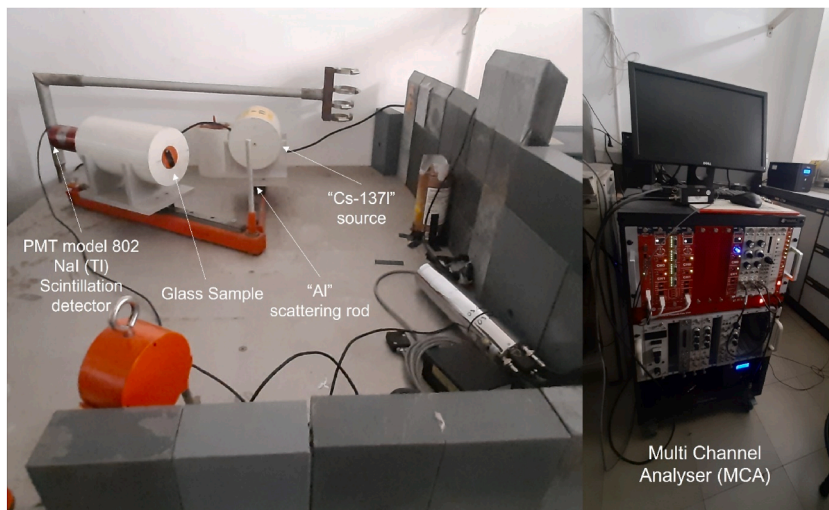
Fig. 7. Photograph of the instrument used to obtain the radiation measurements.

$$B(E, X) = 1 + \frac{b-1}{K-1}(K^x - 1) \; for \; K \neq 1 \tag{11}$$

$$B(E, X) = 1 + (b-1)x \; for \; K = 1 \tag{12}$$

Were,

$$K(E, X) = cx^a + d \frac{tanh\left(\frac{x}{X_K} - 2\right) - tanh(-2)}{1 - tanh(-2)} \; for \; (x) \leq 40 mfp \tag{13}$$

where E is the photon energy, x is the penetration depth in mfp, and K(E, X) is the dose-multiplicative factor.

6.9. Instrument used to obtain the radiation data

The instrument used is shown in Fig. 7 computation used in the present work comprises with the American National Standards and as reported using W. Cheewasukhanont et al. [5] and Limkitjaroenporn et al. [37]. Different parameters, including the mass attenuation coefficient (m), the half-value layer (HVL), the tenth-value layer (TVL), and the lead equivalent thickness, are used to analyse the x-ray shielding properties. Shimadzu model RAD Speed Pro high frequency digital radiography X-ray machine operated in the diagnosis X-ray range (50–120 kVp and 20 mAs) was used to measure the x-ray shielding parameters. The full function meter (RMI 242) with optical fibre was used to detect the incident and attenuated spectra and record the X-ray intensities. The ideal setup distances were 50 cm between the X-ray tube and the glass samples, 30 cm between the detector and the table, and 50 cm between the glass samples and the detector. An energy calibration of the system had proven the efficacy of the x-ray transmission technique. The photon energy ranging from 0.015 MeV to 15 MeV at different penetration depths especially 1, 5, 10, 20, and 40 mfp. The radiation measurements obtained from MAC, Z_{eff}, N_{eff}, HVL, TVL, linear attenuation coefficient, and lead equivalent thickness were analyzed using $\pm 5\%$ error in its values as discussed in the later sections.

7. Analysis of the data

7.1. Total mass attenuation coefficients (MAC)

The total mass attenuation coefficients (MAC) were evaluated using equation (2); theoretical calculations were evaluated using WinXCom program and compared with the experimental values at various photon energy ranging from 0.225 to 0.662 MeV and presented in Fig. 8. The attenuation coefficient shows increasing trend with increase in bismuth content replaced with gadolinium content. The attenuation coefficient value decreases with increase in photon energy (225 keV–662 keV). The mass attenuation coefficient values are shown in Tables 3–5. At lower energy range the difference in their mass attenuation coefficient value is intense whereas at higher energy range no difference was observed with variation in bismuth content.

7.2. Effective atomic number (Z_{eff})

The Z_{eff} values are plotted against photon energy and evaluated using equation (4) which is shown in Fig. 9. The result shown in Fig. 9 represents that the effective atomic number value increases with increase in bismuth in replacement of gadolinium content as
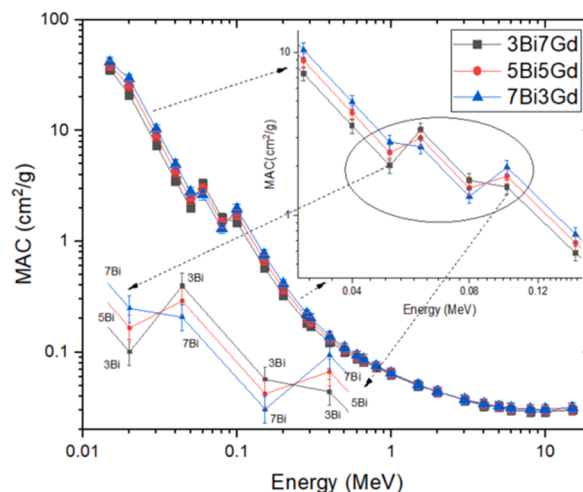

Fig. 8. Mass attenuation coefficient (MAC) bismuth-gadolinium borate glasses.

Table 3

Mass attenuation coefficient (MAC), Effective atomic density (Z_{eff}), and Effective electron density (N_{eff}) of the prepared $75B_2O_3+15Na_2O+3Bi_2O_3+7Gd_2O_3$ glasses.

Energy (keV)	Theoretical			Experiment		
	Mth	Zeff	Neff	Mex	Zeff	Neff
225	0.270961	13.8	4E+23	0.2743	13.969	4E+23
252	0.22079	13.511	4E+23	0.2202	13.476	4E+23
288	0.183793	13.227	4E+23	0.1808	13.009	4E+23
338	0.147766	12.86	4E+23	0.1470	12.79	4E+23
402	0.124707	12.572	4E+23	0.1253	12.63	4E+23
480	0.104777	12.288	4E+23	0.1068	12.529	4E+23
564	0.092518	12.108	3E+23	0.0930	12.172	3E+23
662	0.082315	11.96	3E+23	0.0813	11.813	3E+23

Table 4

Mass attenuation coefficient (MAC), Effective atomic density (Z_{eff}), and Effective electron density (N_{eff}) of the prepared $75B_2O_3+15Na_2O+5Bi_2O_3+5Gd_2O_3$ glasses.

Energy (keV)	Theoretical			Experiment		
	Mth	Zeff	Neff	Mex	Zeff	Neff
225	0.303925	15.479	4E+23	0.2994	15.248	4E+23
252	0.244741	14.977	4E+23	0.2447	14.977	4E+23
288	0.201228	14.482	4E+23	0.1989	14.317	4E+23
338	0.1591	13.846	4E+23	0.1620	14.098	4E+23
402	0.132395	13.347	4E+23	0.1330	13.406	4E+23
480	0.109628	12.857	4E+23	0.1082	12.693	4E+23
564	0.095856	12.545	4E+23	0.0963	12.603	4E+23
662	0.084584	12.29	4E+23	0.0851	12.372	4E+23

Table 5

Mass attenuation coefficient (MAC), Effective atomic density (Z_{eff}), and Effective electron density (N_{eff}) of the prepared $75B_2O_3+15Na_2O+7Bi_2O_3+3Gd_2O_3$ glasses.

Energy (keV)	Theoretical			Experiment		
	Mth	Zeff	Neff	Mex	Zeff	Neff
225	0.335616	17.093	5E+23	0.3355	17.086	5E+23
252	0.267767	16.386	5E+23	0.2718	16.635	5E+23
288	0.21799	15.688	5E+23	0.2178	15.674	5E+23
338	0.169995	14.794	4E+23	0.1719	14.964	4E+23
402	0.139786	14.092	4E+23	0.1412	14.238	4E+23
480	0.114291	13.404	4E+23	0.1158	13.585	4E+23
564	0.099064	12.965	4E+23	0.0984	12.878	4E+23
662	0.086766	12.607	4E+23	0.0875	12.709	4E+23

observed in mass attenuation coefficient. The effective atomic number value decreases with increase in photon energy (225 keV–662 keV). The effective atomic number values are shown in Tables 3–5. The addition of higher 'z' atomic bismuth oxide in replacement of gadolinium oxide content shows better photon absorption in the lower energy range than compared to higher energy range.

7.3. Effective electron density (N_{eff})

The N_{eff} values are plotted against photon energy and evaluated using equation (5) which is shown in Fig. 10. The result shown in Fig. 10 represents that the effective electron number value increases with increase in bismuth in replacement of gadolinium content as observed in effective atomic number. The effective electron density values are shown in Tables 3–5. The effective electron density value decreases with increase in photon energy (225 keV–662 keV). Due to higher electronic cloud in the higher bismuth oxide (Bi_2O_3) content show better electron photon absorption in the lower energy range than at higher energy range.

7.4. Half value layer (HVL)

The half value layer (HVL) defines the quantity to investigate γ-rays shielding potential of a material and the thickness that reduces the incident beam intensity by half value. Fig. 11 display the half value layer for the present glass system using equation (4). It is observed that the HVL values show decreasing trend at higher energy region with replacement of Gd_2O_3 to Bi_2O_3 content. The
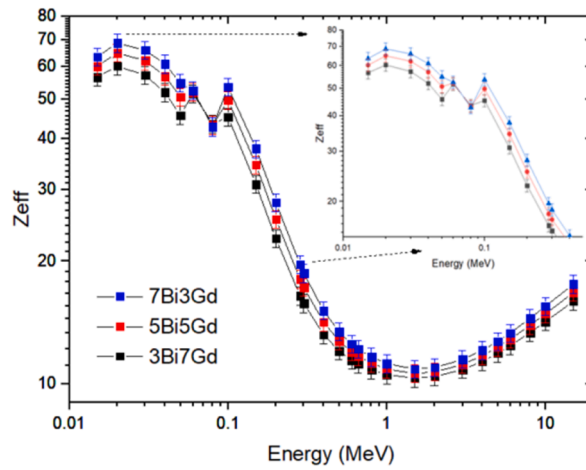
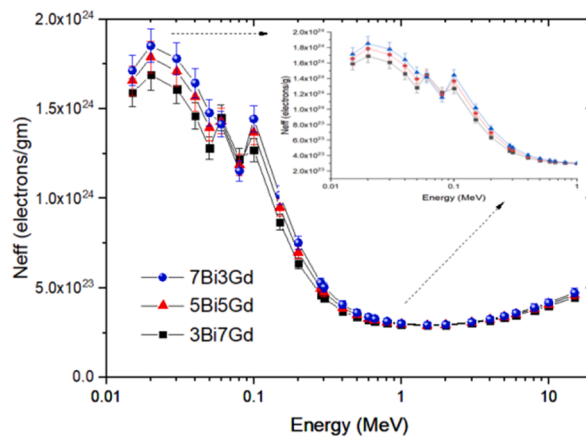**Fig. 9.** Effective atomic density (Z_{eff}) of bismuth-gadolinium borate glasses.

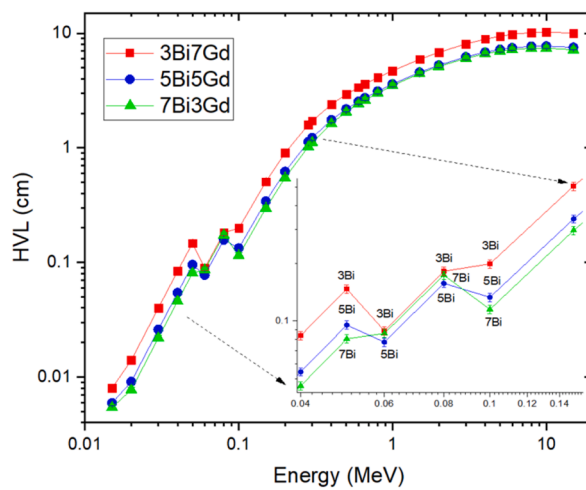**Fig. 10.** Effective electron density (N_{eff}) of bismuth-gadolinium borate glasses.

Fig. 11. Half value layer (HVL) of bismuth-gadolinium borate glasses.

decreasing trend in HVL is due to increase in their density as increased with Bi_2O_3 content as observed in the section.4 (Table 1).

7.5. Tenth value layer (TVL)

The tenth value layer (TVL) defines the quantity to investigate γ-rays shielding potential of a material and the thickness that reduces the incident beam intensity by 1/10th value. Fig. 12 display the tenth value layer for the present glass system using equation (7). It is observed that the TVL values show similar decreasing trend as observed in HVL at higher energy region with replacement of Gd_2O_3 to Bi_2O_3 content.

7.6. Lead equivalent thickness

The lead equivalent thickness defines the thickness of (pb) required to achieve the same shielding effect against the high energy radiation as discussed in equation (8) using linear attenuation coefficient. Fig. 13(a) shows the linear attenuation coefficient against photon energy ranging from 225 to 662 keV. The higher value of linear attenuation coefficient was observed at lower energy regime (less than 400 keV) and values showed higher for higher concentration of bismuth content in the present glasses. Fig. 13(b) shows the lead equivalent thickness against photon energy showing large difference when compared with 3 mol% and 5 mol% of Bi_2O_3 content suggesting that the lead equivalent thickness of the present glasses with ~5 mm thickness. Also, the values show better values (lowest) for higher concentration of bismuth content (7 mol%) suggesting higher Bi_2O_3 content show better shielding ability.

7.7. Equivalent atomic number (Z_{eq})

The Z_{eq} defines the multiple scattering phenomena observed in the glasses using Compton scattering regime. Z_{eq} is one of the vital shielding parameters to evaluate for understanding build-up phenomenon through Compton scattering. The value obtained using Z_1 and Z_2 (atomic numbers) corresponding to R_1 and R_2 ratios as shown in equation (9). The ratio R_1 and R_2 are evaluated using $R = \frac{\mu/\rho_{Compton}}{\mu/\rho_{Total}}$ at a particular energy. These ratios and 'Z_{eq}' values are used to determine the geometric progression (GP) fitting parameters corresponding to atomic numbers Z_1 and Z_2 respectively at a particular energy. The values are obtained using equation (9) and the values are plotted against photon energy and shown in 2D (Fig. 14(a)) and 3D (Fig. 14(b)). At lower energy regime (less than 0.1 MeV) the lowest bismuth content shows higher Z_{eq} value indicating photopeak. Interestingly the photopeak is due to higher luminescence observed at 3 mol% Gd_2O_3 content which is explained in the later section.8. Whereas, at intermediate energy regime (0.1–1.0 MeV) all the glasses show higher Z_{eq} values indicating dominating Compton scattering phenomenon in all the prepared glasses. Also, it is evident that higher concentration of bismuth content (7 mol%) show higher Z_{eq} values suggesting higher Compton scattering phenomenon when compared to other concentrations. Also, at higher energy regime (>2 MeV) the Z_{eq} values decreases with increase in energy suggesting no pair production process play significant in role in the prepared glasses.

7.8. Build-up factor and exposure build-up factor

The build-up is defined as the ratio of the total value of a specified radiation quantity at any point to the contribution to that value from radiation that arrives at the point without colliding. There are two types of build-up factors: (a) the absorbed or deposited energy in the interacting materials, and the detector response function is that of absorption in the interacting medium (BF); and (b) the
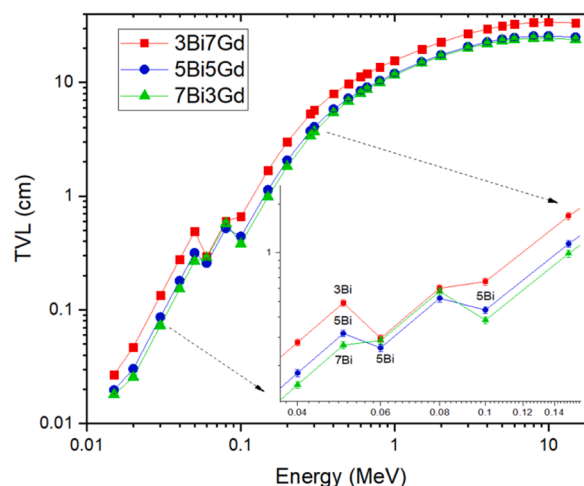

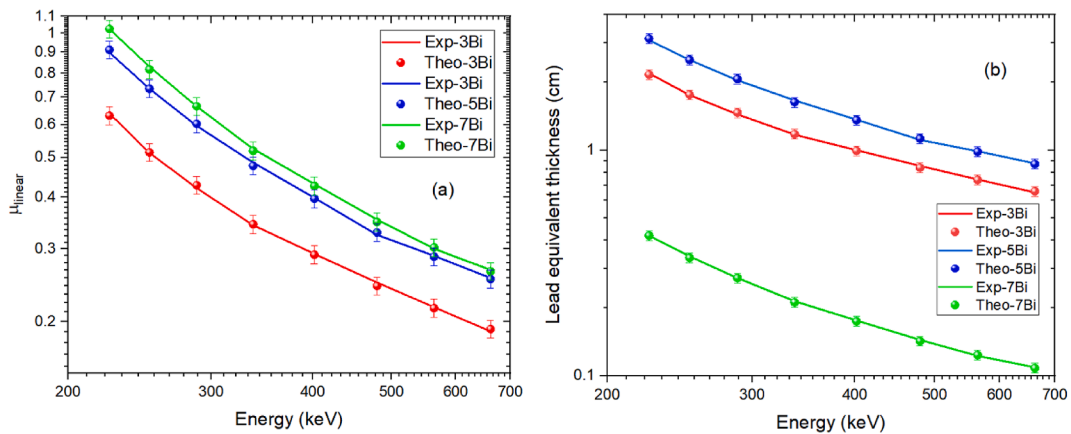**Fig. 12.** Tenth value layer (TVL) of bismuth-gadolinium borate glasses.

Fig. 13. (a) Linear attenuation coefficient (μ_{linear}) (b) Lead equivalent thickness (cm) of bismuth-gadolinium borate glasses.
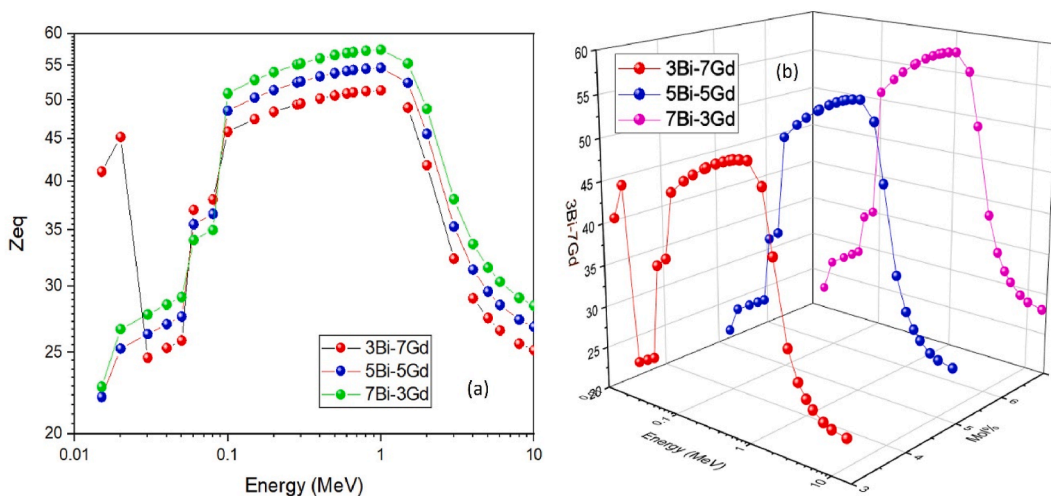

Fig. 14. Equivalent atomic number (Z_{eq}) of bismuth-gadolinium borate glasses. (a) 2D graph (b) 3D graph.

exposure absorption build-up factor (EABF), in which the quality of interest is the exposure, and the detector response function is that of absorption in air (Harima, 1993). Build-up factor and Exposure build-up factor evaluated using the geometric progression (GP) fitting method (ANSI/ANS-6.4.3–1991) using equations (10)–(13). These values are evaluated and shown in Tables 6–8 for the present glass samples by applying GP fitting parameters (*b, c, a, X_K,* and *d*) to an infinite homogenous medium with an optical thickness range of 1–40 mean free path (mfp) source to detector distance, these parameters are vital to understand the material absorbed dose, and radiation shielding ability. Fig. 15 shows the build-up factor (BF) against photon energy (MeV) for prepared glass samples 3Bi-7Gd (Fig. 15(a)), 5Bi-5Gd (Fig. 15(b)), and 7Bi-3Gd (Fig. 15(c)).

Fig. 16 shows the 3D and 2D comparison graph of build-up factor at 40 mean free path (mfp). The comparison graph clearly suggests that the BF was compared at penetration depth at 40mfp for the energy ranging from 0.015 to 15 MeV for various concentration of Bi_2O_3 content in replacement of Gd_2O_3 in the prepared glass samples. Fig. 16 shows clear difference in their build-up factor values with various concentration of Bi_2O_3 content in the glass samples. At lower energy range (Region: I, less than 0.1 MeV) showing photopeak arising due to photo-absorption effect proportional to Z^{4-5} and $1/E^{3.5}$ [38]. At the intermediate energy regime (Region: II, less than 0.1–1.0 MeV), the Compton scattering dominates significantly due to more scattering phenomenon in the present glasses. The primary method of photon interaction, known as Compton scattering, only aids in the degradation of photon energy due to scattering and is unable to eliminate the photon [39].

7.8.1. Region: I

At this region the build-up factor values show increasing trend with increase in Bi_2O_3 content. Interestingly at higher concentration of Bi_2O_3 (7 mol%) and lower content of Gd_2O_3 (3 mol%) the build-up factor at 40 mfp is higher due to at this energy regime (Region I) the photopeak dominates in the present glasses as discussed in section.7.

Table 6

Build-up factor (BF) and Exposure build-up factor (EABF) G-P fitting coefficients (*b, c, a, X_K,* and *d*) of $75B_2O_3+15Na_2O+3Bi_2O_3+7Gd_2O_3$ glass.

Energy (MeV)	Z_{eq}	Build-up factor					Exposure Build-up factor				
		b	c	a	Xk	d	b	c	a	Xk	d
0.015	21.55116	1.006	0.863	−0.133	8.547	0.180	1.006	0.871	−0.143	6.623	0.193
0.02	44.72882	1.009	0.371	0.258	14.201	−0.160	1.009	0.376	0.252	14.267	−0.153
0.03	24.81243	1.032	0.326	0.249	17.797	−0.183	1.033	0.374	0.196	26.164	−0.282
0.04	25.55344	1.063	0.334	0.246	13.924	−0.131	1.063	0.338	0.247	11.810	−0.120
0.05	26.14474	1.103	0.344	0.243	14.323	−0.136	1.098	0.365	0.233	13.953	−0.136
0.06	36.89245	1.061	0.447	0.185	13.906	−0.098	1.054	0.489	0.163	14.008	−0.080
0.08	37.9408	1.129	0.283	0.335	13.483	−0.231	1.099	0.370	0.252	13.390	−0.163
0.1	45.46851	1.141	0.249	0.353	13.012	−0.232	1.112	0.307	0.303	13.050	−0.192
0.15	46.85694	1.264	0.425	0.218	13.227	−0.133	1.155	0.574	0.129	13.551	−0.064
0.2	47.59773	1.440	0.527	0.168	14.523	−0.094	1.259	0.554	0.145	14.616	−0.077
0.3	48.40341	1.993	0.472	0.207	14.106	−0.140	1.429	0.673	0.104	14.352	−0.065
0.4	48.82265	2.269	0.601	0.147	13.895	−0.104	1.543	0.790	0.064	14.173	−0.042
0.5	49.09296	2.364	0.710	0.107	13.903	−0.088	1.613	0.884	0.040	13.906	−0.035
0.6	49.21271	2.405	0.776	0.083	13.784	−0.073	1.652	0.935	0.026	13.913	−0.028
0.8	49.37368	2.337	0.856	0.056	13.750	−0.057	1.676	0.997	0.008	13.878	−0.018
1	49.44265	2.238	0.905	0.040	13.526	−0.046	1.678	1.024	0.001	13.568	−0.015
1.5	49.60196	1.928	1.032	0.000	13.237	−0.018	1.614	1.086	−0.015	12.402	−0.005
2	41.4849	1.859	1.035	0.005	13.096	−0.027	1.630	1.098	−0.013	12.293	−0.013
3	32.57954	1.678	1.012	0.012	12.594	−0.030	1.601	1.054	−0.001	12.452	−0.020
4	29.09784	1.542	1.015	0.010	14.075	−0.029	1.546	1.022	0.009	12.924	−0.026
5	27.5402	1.463	0.982	0.021	14.145	−0.038	1.481	1.008	0.014	13.194	−0.029
6	26.61211	1.391	0.978	0.023	14.324	−0.038	1.439	0.983	0.023	13.340	−0.036
8	25.65925	1.301	0.957	0.033	13.919	−0.044	1.355	0.972	0.029	13.643	−0.042
10	25.20212	1.240	0.951	0.038	14.227	−0.049	1.299	0.947	0.041	13.926	−0.054
15	24.89394	1.151	0.955	0.045	14.603	−0.051	1.202	0.950	0.049	14.294	−0.059

Table 7

Build-up factor (BF) and Exposure build-up factor (EABF) G-P fitting coefficients (*b, c, a, X_K,* and *d*) of $75B_2O_3+15Na_2O+5Bi_2O_3+5Gd_2O_3$ glass.

Energy (MeV)	Z_{eq}	Build-up factor					Exposure Build-up factor				
		b	c	a	Xk	d	b	c	a	Xk	d
0.015	41.92032	1.005	0.356	0.279	13.548	−0.174	1.005	0.386	0.246	15.020	−0.147
0.02	25.36219	1.011	0.269	0.312	17.561	−0.284	1.012	0.153	0.585	11.670	−0.572
0.03	26.45781	1.025	0.326	0.251	17.662	−0.189	1.027	0.372	0.192	26.568	−0.274
0.04	27.25877	1.046	0.322	0.253	13.946	−0.133	1.051	0.333	0.244	12.862	−0.109
0.05	27.88809	1.083	0.350	0.243	13.431	−0.139	1.081	0.358	0.239	13.291	−0.139
0.06	35.56487	1.070	0.431	0.195	14.001	−0.106	1.063	0.470	0.174	13.937	−0.088
0.08	36.60184	1.145	0.298	0.319	13.604	−0.216	1.111	0.380	0.244	13.467	−0.156
0.1	48.15949	1.130	0.247	0.347	12.999	−0.216	1.115	0.260	0.341	13.086	−0.212
0.15	49.7432	1.177	0.498	0.157	13.432	−0.080	1.108	0.635	0.094	13.863	−0.038
0.2	50.59085	1.309	0.595	0.128	14.656	−0.068	1.226	0.535	0.153	14.592	−0.080
0.3	51.54024	1.860	0.448	0.218	14.095	−0.145	1.383	0.650	0.112	14.353	−0.069
0.4	52.04832	2.148	0.569	0.158	13.855	−0.109	1.495	0.758	0.074	14.122	−0.046
0.5	52.37656	2.269	0.683	0.117	13.892	−0.093	1.565	0.851	0.048	13.942	−0.037
0.6	52.55967	2.346	0.747	0.091	13.769	−0.076	1.606	0.906	0.033	13.913	−0.030
0.8	52.77825	2.308	0.835	0.062	13.803	−0.061	1.638	0.973	0.014	13.855	−0.020
1	52.8543	2.227	0.883	0.046	13.488	−0.049	1.646	1.008	0.005	13.598	−0.016
1.5	51.19149	1.932	1.023	0.003	13.288	−0.019	1.605	1.079	−0.014	12.447	−0.006
2	45.21503	1.865	1.016	0.011	13.963	−0.033	1.602	1.087	−0.010	12.562	−0.014
3	35.51076	1.682	0.991	0.020	12.833	−0.039	1.589	1.050	0.001	12.631	−0.025
4	31.45555	1.547	0.991	0.020	13.955	−0.040	1.538	1.018	0.012	13.008	−0.031
5	29.59862	1.446	0.997	0.018	14.152	−0.037	1.481	1.004	0.017	13.280	−0.033
6	28.53621	1.383	0.983	0.023	14.304	−0.039	1.430	0.993	0.021	13.251	−0.037
8	27.35958	1.293	0.963	0.033	14.315	−0.046	1.354	0.967	0.033	13.580	−0.048
10	26.8073	1.230	0.964	0.036	14.312	−0.048	1.277	0.952	0.042	14.071	−0.055
15	26.44536	1.147	0.955	0.048	14.640	−0.055	1.198	0.959	0.049	14.387	−0.060

7.8.2. Region: II

At region: II, the build-up factor values show decreasing trend with increase in Bi_2O_3 content. The scattering phenomenon dominates at this region and one can observe from 3D (Fig. 16(a)) and 2D (Fig. 16(b)) graph that beyond 0.1 MeV energy a clear switch over of build-up factor values is observed. Such decrease in trend in the build-up factor is due to the 3D lattice constants (a, b, c) for the Bi_2O_3 cubic structure as shown in Fig. 17 (a) [40] is greater than Gd_2O_3 cubic structure [41] as shown in Fig. 17(b).

Table 8

Build-up factor (BF) and Exposure build-up factor (EABF) G-P fitting coefficients (*b, c, a, X$_K$,* and *d*) of $75B_2O_3+15Na_2O+7Bi_2O_3+3Gd_2O_3$ glass.

Energy (MeV)	Z_{eq}	Build-up factor					Exposure Build-up factor				
		b	c	a	Xk	d	b	c	a	Xk	d
0.015	22.87823	1.005	1.085	−0.267	7.609	0.235	1.005	1.091	−0.274	6.297	0.243
0.02	26.74989	1.009	0.251	0.351	16.759	−0.351	1.010	0.194	0.525	12.101	−0.498
0.03	27.91855	1.020	0.352	0.249	13.912	−0.182	1.028	0.374	0.190	29.340	−0.317
0.04	28.76273	1.040	0.387	0.201	24.583	−0.277	1.063	0.338	0.247	11.810	−0.120
0.05	26.43002	1.100	0.345	0.243	14.173	−0.136	1.098	0.365	0.233	13.953	−0.136
0.06	34.20697	1.080	0.414	0.205	14.102	−0.115	1.054	0.489	0.163	14.008	−0.080
0.08	35.214	1.162	0.314	0.302	13.735	−0.201	1.099	0.370	0.252	13.390	−0.163
0.1	50.58572	1.152	0.227	0.369	13.111	−0.203	1.112	0.307	0.303	13.050	−0.192
0.15	52.3091	1.170	0.447	0.189	13.278	−0.101	1.155	0.574	0.129	13.551	−0.064
0.2	53.25402	1.489	0.289	0.324	14.124	−0.185	1.259	0.554	0.145	14.616	−0.077
0.3	54.27867	1.859	0.403	0.248	14.056	−0.165	1.429	0.673	0.104	14.352	−0.065
0.4	54.8462	2.132	0.518	0.185	13.802	−0.126	1.543	0.790	0.064	14.173	−0.042
0.5	55.223	2.260	0.624	0.140	13.877	−0.104	1.524	0.822	0.056	14.034	−0.039
0.6	55.42237	2.242	0.707	0.106	13.780	−0.084	1.568	0.881	0.039	13.937	−0.032
0.8	55.67482	2.234	0.798	0.073	13.637	−0.065	1.606	0.951	0.019	13.831	−0.022
1	55.8105	2.158	0.862	0.053	13.570	−0.053	1.619	0.995	0.008	13.636	−0.017
1.5	54.16915	1.934	0.998	0.010	13.323	−0.023	1.589	1.065	−0.011	12.559	−0.007
2	48.49504	1.822	0.990	0.018	13.311	−0.037	1.578	1.077	−0.008	12.707	−0.016
3	38.24204	1.686	0.973	0.026	13.039	−0.047	1.579	1.046	0.003	12.785	−0.028
4	33.80705	1.551	0.968	0.029	13.844	−0.050	1.531	1.014	0.015	13.086	−0.036
5	31.62264	1.485	0.952	0.036	14.066	−0.054	1.490	0.992	0.022	13.346	−0.040
6	30.41938	1.402	0.958	0.034	14.257	−0.051	1.422	1.002	0.020	13.169	−0.038
8	29.12042	1.291	0.957	0.037	14.052	−0.050	1.344	0.987	0.028	13.706	−0.045
10	28.44161	1.228	0.958	0.040	14.319	−0.053	1.292	0.954	0.044	14.097	−0.061
15	28.00739	1.144	0.948	0.054	14.753	−0.060	1.193	0.969	0.049	14.500	−0.061

7.8.3. Region: III

At this region, the pair production phenomenon dominates beyond 3 MeV, it is visible that the build-up factor value switches over again as seen in region I. The values increase with increase in concentration of Bi_2O_3 content. Such increase in the values suggests that the values are proportional to Z^2 and log E [38].

The exposure build-up factor (EABF) vs photon energy is shown in Fig. 18(a–c). Representing 3Bi-7Gd (Fig. 18(a)), 5Bi-5Gd (Fig. 18 (b)), and 7Bi-3Gd (Fig. 18(c)). The EABF show similar trend as observed in the build-up factor.

The exposure build-up factor values show very similar trend as observed in build-up factor as shown in Fig. 18(a–c). In Fig. 19(a and b) shows 3D and 2D graphs of the regions I and II show increasing trend with increase in Bi_2O_3 content due to at these regions they are proportional to z factor [42]. Whereas in the region III it decreases with increase in Bi_2O_3 content at intermediate region as observed in build-up factor.

8. Contrast and discussion

It is found that the present work (PW) shows the mass attenuation coefficient at 0.02 MeV and 10 MeV for the present synthesised glasses compared with other reported glasses as shown in Table 9. It is observed that lowest mass attenuation coefficient was observed for 3Bi-7Gd glasses than compared to 5Bi-5Gd and 7Bi-3Gd glasses. It is also noted that 3Bi-7Gd glass show higher values than other reported literatures at 0.02 MeV. Whereas show almost same values at higher energy range (10 MeV) when compared to other reported literature. The present synthesised glasses with other reported glasses were compared with effective electron density, effective atomic density, half value layer, tenth value layer at 0.02 and 10 MeV as shown in Table 10. It is observed that the present work (PW) shows almost similar values and comparable as observed in the other reported glasses.

The present glasses were compared with commercially available glasses and found that these glasses find potential use in safety or protective glasses from harmful radiations. When compared at 0.06 MeV of the commercial glasses such as RS-360, RS253-G18, Hematite-Serpentine, and Ordinary concrete they show HVL values around 0.09427, 0.60333, 1.13467, and 1.21838 [45,46]. The present glasses show HVL values around 0.089, 0.077, 0.086 for 3Bi-7Gd, 5Bi-5Gd, and 7Bi-3Gd glasses respectively. Which suggests that the present prepared glasses show lower than the available commercial glasses making them potential candidates. The radiation attenuation capacities such as lead equivalent (Zeq), build up factor, and exposure buildup factor for the present glasses show higher values at lower and higher energy region when compared with TiO_2–P_2O_5–Li_2O glasses [47] and higher than APPV5.0 [44]. As a result of the obtained data, it is concluded that increase in density would lead to enhance the property of shielding mechanism hence in the present case the 3Bi-7Gd glasses are prominent for radiation shielding behaviour and can be used as shielding glasses in X-ray/γ-ray radiation imaging rooms in medical research laboratories.

9. Photoluminescence of Gd^{3+} ions

The photoluminescence spectra of the prepared samples are shown in Fig. 20. The excitation spectra (Fig. 20(a)) show higher
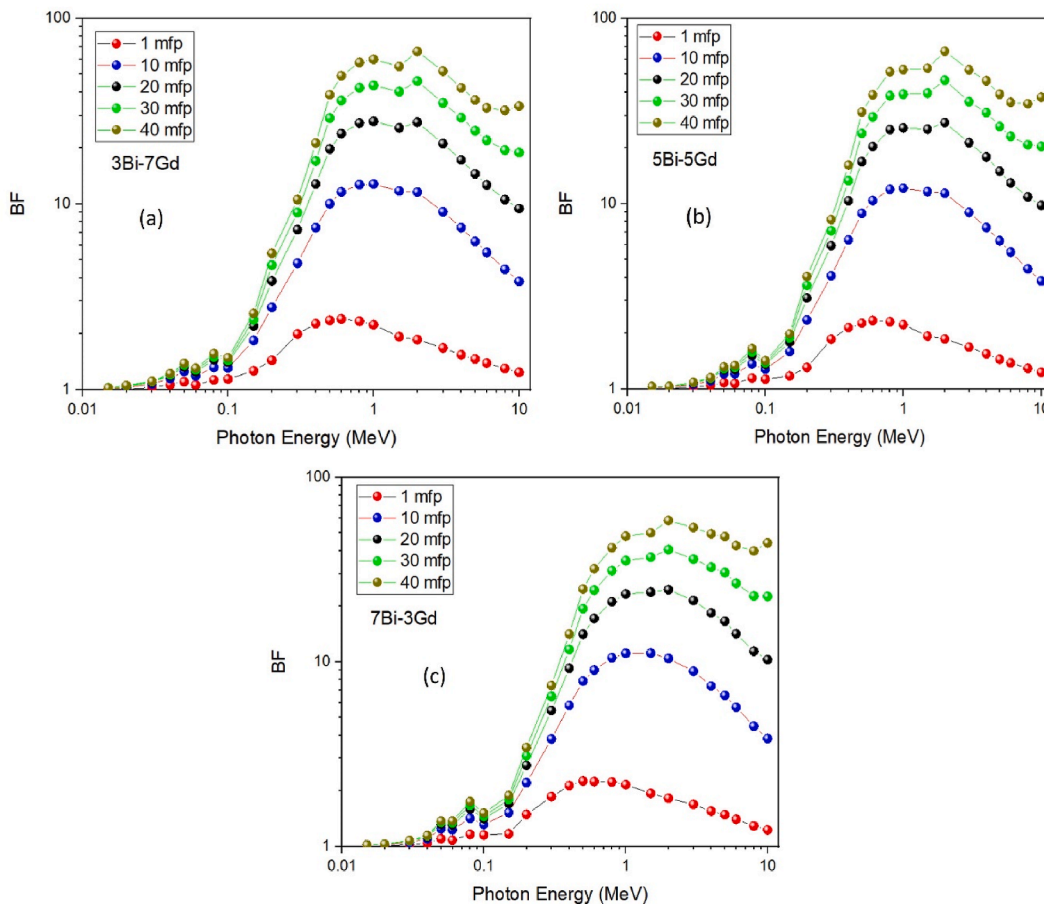
Fig. 15. Build-up factor (BF) of bismuth-gadolinium borate glasses. (a) 3Bi-7Gd (b) 5Bi-5Gd (c) 7Bi-3Gd Glass samples.
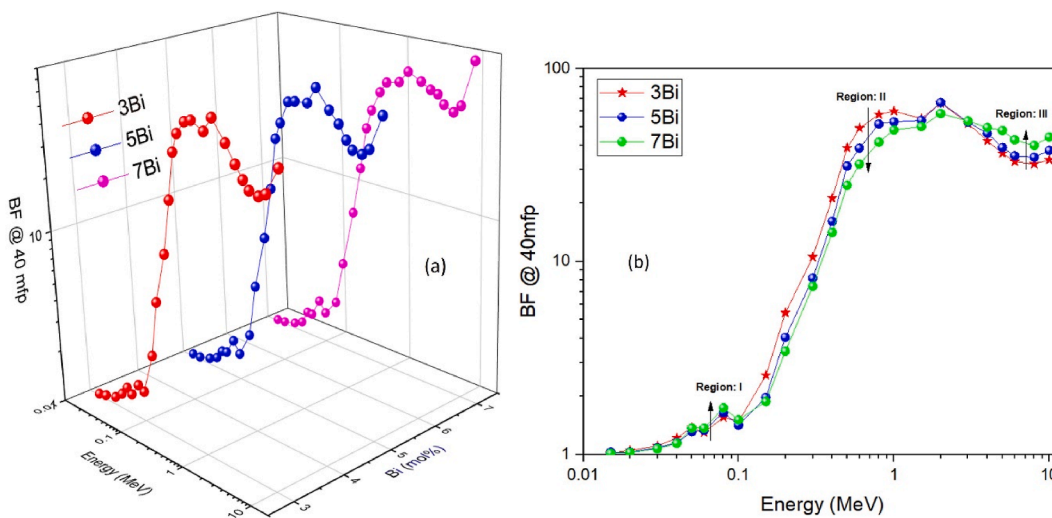

Fig. 16. (a) 3D and (b) 2D comparison graph of build-up factor at 40 mean free path(mfp) for the present glass samples.

intensity at 275 nm (transition of $^8S_{7/2} \rightarrow {}^6I_J$). From ^6I_J level to ^6P_J transition the electrons undergo non-radiative transition (NR). The luminescence intensity at 311 nm (transition of $^6P_J \rightarrow {}^8S_{7/2}$) [48–51] show radiative transition which increases with increase in Gd_2O_3 content as shown in Fig. 20(b). The energy level diagram for the present glasses is displayed in Fig. 21. The photopeak shows higher at
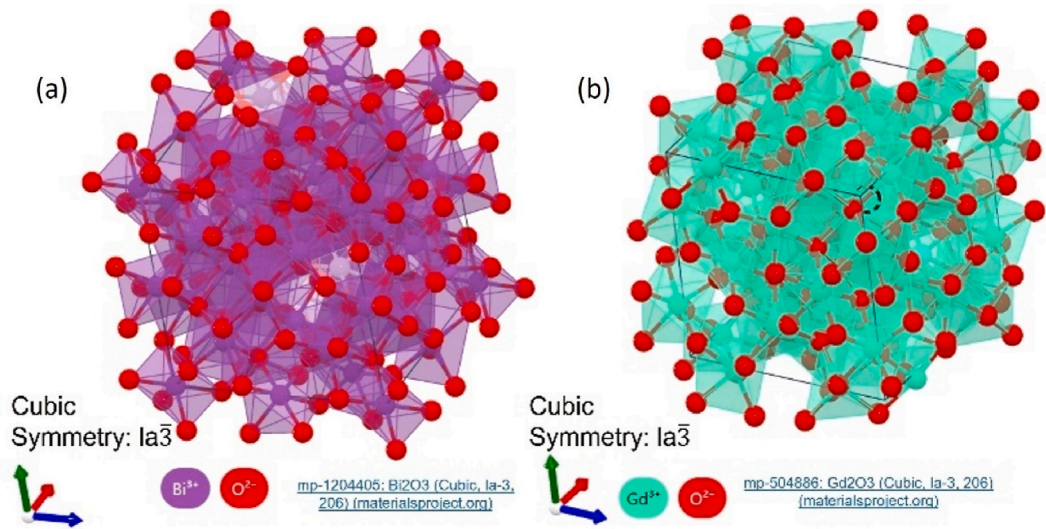
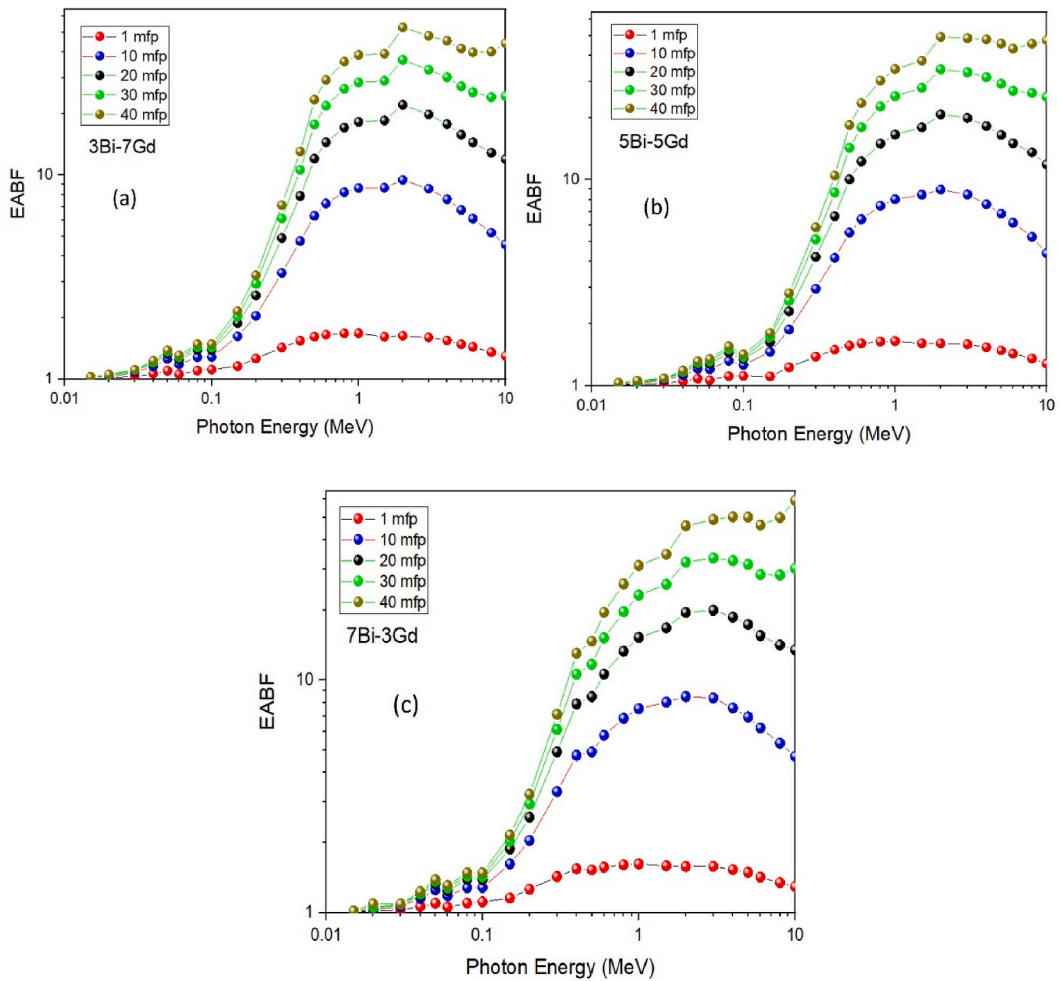**Fig. 17.** (a) Bi_2O_3 and (b) Gd_2O_3 cubic structure.

Fig. 18. Exposure absorption build-up factor (EABF) of bismuth-gadolinium borate glasses. (a) 3Bi-7Gd (b) 5Bi-5Gd (c) 7Bi-3Gd Glass samples.
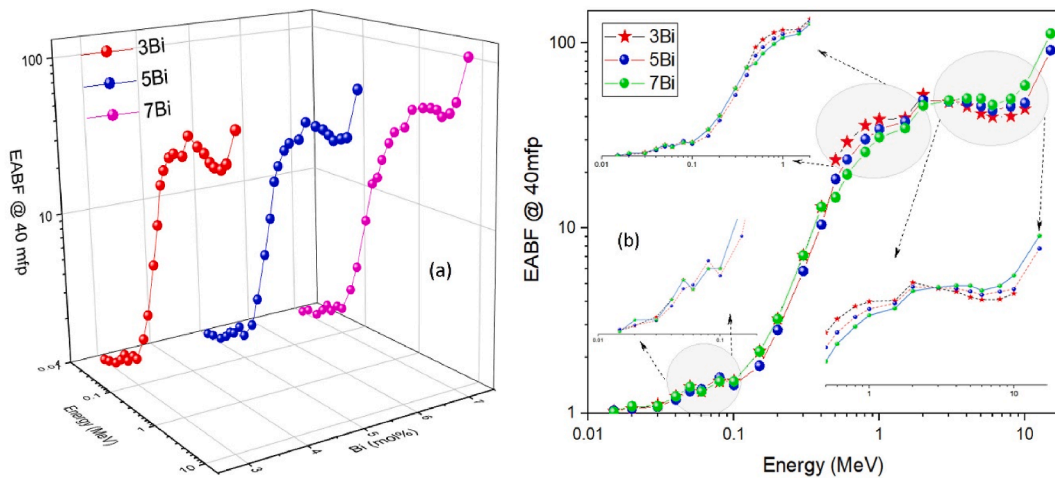
Fig. 19. Exposure absorption build-up factor (EABF) of bismuth-gadolinium borate glasses at 40 *mfp*. (a) 3D (b) 2D graph.

Table 9
Comparison of present work with other reported glasses for Mass attenuation coefficient (MAC) at 0.02 and 10 MeV.

Glass samples	Density (g/cm³)	MAC (MeV)		Observations on glasses		Ref
		0.02	10	at 0.02 MeV	at 10 MeV	
3Bi-7Gd	2.3302	21.206	0.0290	–	–	PW
5Bi-5Gd	2.9992	25.3842	0.0298	–	–	PW
7Bi-3Gd	3.0526	29.3974	0.0306	–	–	PW
PT1	5.371	27.142	0.037	7Bi-3Gd > PT1	PT1 > 7Bi-3Gd	[34]
PTZ1	6.257	19.199	0.035	7Bi-3Gd > PTZ1	PTZ1 > 7Bi-3Gd	[34]
SLGC-E4	3.43	12.153	0.029	SLGC-E4 > PW	PW > SLGC-E4	[35]
SLGC-E5	3.51	12.998	0.029	SLGC-E5 > PW	PW > SLGC-E5	[35]
G5	4.15	6.275	0.025	PW > G5	PW > G5	[43]
$5Bi_2O_3$–$61B_2O_3$–$5Al_2O_3$–$29Na_2O$ (a)	–	5.059	0.022	PW > (a)	PW > (a)	[43]
$5PbO$–$25SiO_2$-46.67B_2O_3-23.33Na_2O (b)	–	5.167	0.021	PW > (b)	PW > (b)	[43]
49.46SiO_2- 26.38Na_2O- 23.08CaO- 1.07P_2O_5 (c)	–	3.982	0.024	PW > (c)	PW > (c)	[43]
APPV5.0 (d)	5.834	44.364	0.033	PW < (d)	PW < (d)	[44]

*PW = Present Work; (a) = $5Bi_2O_3$–$61B_2O_3$–$5Al_2O_3$–$29Na_2O$; (b) = $5PbO$–$25SiO_2$-46.67B_2O_3-23.33Na_2O; (c) = 49.46SiO_2- 26.38Na_2O- 23.08CaO-1.07P_2O_5; (d) = APPV5.0.

Table 10
Comparison of present work with other reported glasses for Effective electron density, effective atomic density, half value layer, tenth value layer at 0.02 and 10 MeV.

Glass samples	N_{eff} electrons/gm $\times 10^{24}$		Z_{eff}		HVL (cm)		TVL (cm)		Ref
	0.02 MeV	10 MeV	0.02 MeV	10 MeV	0.02 MeV	10 MeV	0.02 MeV	10 MeV	
3Bi-7Gd	1.690	3.990	60.313	14.232	0.014	10.232	0.047	33.98	PW
5Bi-5Gd	1.787	4.091	65.008	14.878	0.0091	7.731	0.030	25.68	PW
7Bi-3Gd	1.852	4.183	68.715	15.519	0.0077	7.401	0.025	24.58	PW
PT1	–	–	68	32	0.006	3.45	–	–	[34]
PTZ1	–	–	50	30	0.01	3.0	–	–	[34]
SLGC-E4	0.99	0.4	40	14	0.005	6.98	–	–	[35]
SLGC-E5	1.01	0.39	44	15	0.005	6.75	–	–	[35]
APPV5.0			37.80	29.69	0.003	3.5			[44]

lower concentration of Bi_2O_3 content and higher concentration of Gd_2O_3 content. Such photo-peak observed in luminescence spectra reflects in their radiation shielding measurements (γ-rays as source).

10. Conclusions

Bismuth gadolinium sodium borate glasses were synthesised using melt-quenching technique. The measurements were evaluated and obtained for several shielding parameters using Phy-X/WinXCom software in the photon energy range (0.15–15 MeV). With
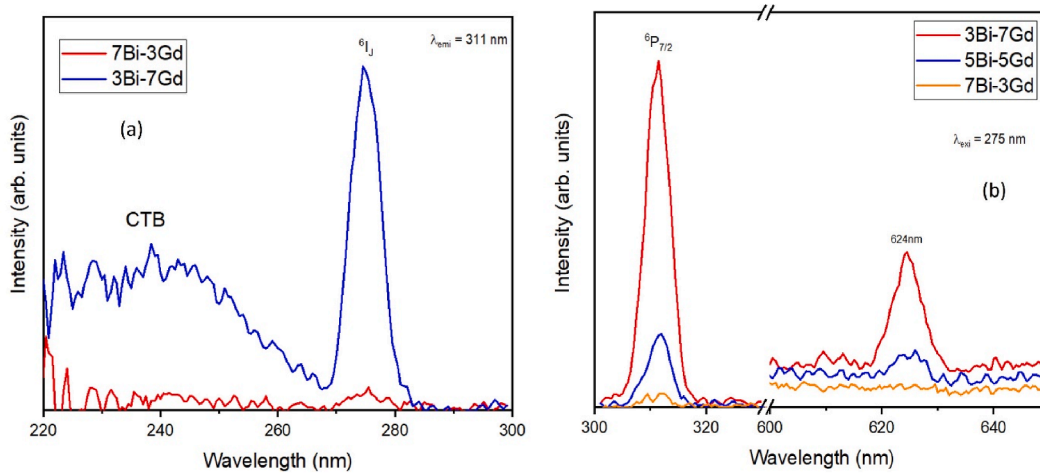
Fig. 20. (a) Photoluminescence excitation and (b) Emission spectra of the prepared bismuth-gadolinium borate glasses.
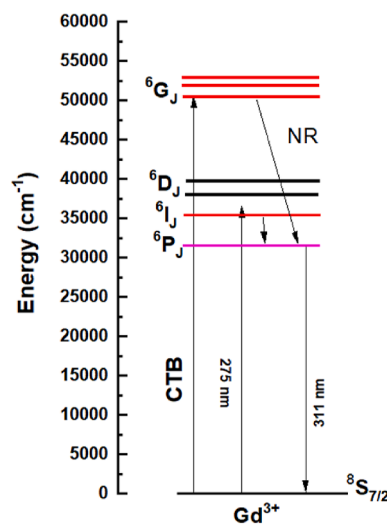

Fig. 21. Energy level diagram of bismuth-gadolinium borate glasses.

addition of Bi_2O_3 content the density increases ranging from 2.330 to 3.052 g/cm^3 whereas molar volume decreases from 43.61 to 34.64. Optical transmittance in the prepared glass samples is more than $\geq$72% in its visible region. The trend observed in optical Tauc band gap and ASF band gap values similar. With increasing photon energy (MeV), the mass attenuation coefficient (MAC), effective atomic density (Z_{eff}), and effective electron density (N_{eff}) follow a similar pattern. For higher concentrations of bismuth content (7 mol %), lead equivalent and linear attenuation coefficient values are similar and better (lowest). Interestingly, the lead equivalent (Z_{eq}) value shows the photopeak for 3 mol% Bi_2O_3 content. At intermediate energies, Compton scattering dominates for different concentrations of Bi_2O_3 content. Higher Bi_2O_3 content shows better shielding ability making them potential candidate. It has been determined that the build-up and exposure build-up factors have higher values for higher concentrations of Bi_2O_3 content at lower energy regime (<0.1 MeV). Whereas the exponential growth is observed in all concentrations with increase in mean free paths (mfp). In the intermediate energy regime (0.1–1.0 MeV), the buildup factor and exposure buildup factor decrease with increase in Bi_2O_3 content. Interestingly at higher energy regime (>1.0 MeV) the buildup factor and exposure buildup factor increase with increase in Bi_2O_3 content. Photoluminescence study reveal that the lower concentration of Bi_2O_3 (3 mol%) content and higher concentration of Gd_2O_3 (7 mol%) content show higher photo-peak at 311 nm emission (UV range). The data obtained lead to the conclusion that in the present case the 3Bi-7Gd glasses are notable for their radiation shielding behaviour and can be used as shielding glasses in X-ray and gamma-ray radiation imaging rooms as a protecting glass in medical and research laboratories.

Author contribution statement

R. Ruamnikhom: Performed the experiments; Analyzed and interpreted the data; Contributed reagents, materials, analysis tools or

data; Wrote the paper.

R. Rajaramakrishna: Conceived and designed the experiments; Performed the experiments; Analyzed and interpreted the data; Wrote the paper.

W. Chaiphaksa: Performed the experiments; Analyzed and interpreted the data; Wrote the paper.

W. Cheewasukhanont: Analyzed and interpreted the data; Contributed reagents, materials, analysis tools or data.

N. Intachai: Conceived and designed the experiments; Performed the experiments; Analyzed and interpreted the data; Contributed reagents, materials, analysis tools or data.

S. Kothan: Performed the experiments; Analyzed and interpreted the data; Contributed reagents, materials, analysis tools or data.

J. Kaewkhao: Conceived and designed the experiments; Contributed reagents, materials, analysis tools or data.

Data availability statement

Data will be made available on request.

Declaration of competing interest

The authors declare that they have no known competing financial interests or personal relationships that could have appeared to influence the work reported in this paper.

Acknowledgements

References

[1] A. Gharam, a Alharshan, b Canel Eke, M.S. Al-Buriahi, Radiation-transmission and self-absorption factors of P2O5-SrO-Sb2O3 glass system, Radiat. Phys. Chem. 193 (2022), 109938, https://doi.org/10.1016/j.radphyschem.2021.109938.

[2] M.S. Al-Buriahi, D.K. Gaikwad, H.H. Hegazy, Chahkrit Sriwunkum, R. Neffati, Fe-based alloys and their shielding properties against directly and indirectly ionizing radiation by using FLUKA simulations, Phys. Scripta 96 (4) (2021), 045303, https://doi.org/10.1088/1402-4896/abdd52.

[3] K.A. Naseer, S. Arunkumar, K. Marimuthu, J. Non-Cryst. Solids (2019), https://doi.org/10.1016/j.jnoncrysol.2019.119463.

[4] S. Kaewjaeng, S. Kothana, W. Chaiphaksa, N. Chanthima, R. Rajaramakrishna, H.J. Kim, J. Kaewkhao, Radiat. Phys. Chem. 160 (2019) 41–47.

[5] W. Cheewasukhanont, K. Siengsanoh, P. Limkitjaroenporn, W. Chaiphaksa, S. Kothan, N. Intachai, H.J. Kim, J. Kaewkhao, Radiat. Phys. Chem. 201 (2022), 110385.

[6] Mohammed Sultan Al-Buriahi, T. Baris, Tonguc, Applied Physics A 125 (2019) 482, https://doi.org/10.1007/s00339-019-2777-4.

[7] S. ShanmugaSundari, K. Marimuthu, M. Sivraman, S.S. Babu, J. Lumin. 130 (7) (2010) 1313–1319, https://doi.org/10.1016/j.jlumin.2010.02.046.

[8] Q. Chen, K.A. Naseer, K. Marimuthu, P.S. Kumar, B. Miao, K.A. Mahmoud, M.I. Sayyed, J. Australas. Ceram. Soc. (2021), https://doi.org/10.1007/s41779-020-00531-8.

[9] Badriah Albarzan, Aljawhara H. Almuqrin, M.S. Koubisy, E.A. Abdel Wahab, K.A. Mahmoud, KhS. Shaaban, M.I. Sayyed, Prog. Nucl. Energy 141 (November 2021), 103931, https://doi.org/10.1016/j.pnucene.2021.103931.

[10] A.M. Fayad, K.S. Shaaban, W.M. Abd-Allah, et al., J. Inorg. Organomet. Polym. 30 (2020) 5042–5052, https://doi.org/10.1007/s10904-020-01641-3.

[11] S. Ravangvong, N. Chanthima, R. Rajaramakrishna, H.J. Kim, J. Kaewkhao, J. Lumin. 219 (2020), 116950.

[12] Garima, V. Deepak Hebbar, Basavaraj Gurav, J. Kaewkhao, N. Intachai, S. Kothan, R. Rajaramakrishna, Optik - Int. J. Light Electron Optics 262 (2022), 169366.

[13] K.N. Sharvani, S. Ganesh Prasad, J. Kaewkhao, S. Kothan, W. Rachniyom, Altaf Pasha, R. Rajaramakrishna, Radiat. Phys. Chem. 199 (2022), 110295.

[14] A.F.A. El-Rehim, A.M. Ali, H.Y. Zahran, et al., Spectroscopic, structural, thermal, and mechanical properties of B2O3-CeO2-PbO2 glasses, J. Inorg. Organomet. Polym. 31 (2021) 1774–1786, https://doi.org/10.1007/s10904-020-01799-w.

[15] O.I. Sallam, A.M. Madbouly, N.A. Elalaily, F.M. Ezz-Eldin, J. Alloys Compd. 843 (2020), 156056, https://doi.org/10.1016/j.jallcom.2020.156056.

[16] Nimitha S. Prabhu, Vinod Hegde, M.I. Sayyed, O. Agar, Sudha D. Kamath, Mater. Chem. Phys. 230 (2019) 267–276, https://doi.org/10.1016/j.matchemphys.2019.03.074.

[17] Synthesis, optical, structural, and radiation transmission properties of PbO/Bi2O3/B2O3/Fe2O3 glasses: an experimental and in silico study, Opt. Mater. 117 (2021), 111173.

[18] M.S. Al-Buriahi, Z.A. Alrowaili, Sultan J. Alsufyani, I.O. Olarinoye, Abdulaziz N. Alharbi, Chahkrit sriwunkum, and imen kebaili, J. Mater. Sci. Mater. Electron. 33 (3) (2022) 1123–1139, https://doi.org/10.1007/s10854-021-07382-4.

[19] M.S. Al-Buriahi, Radiation shielding performance of a borate-based glass system doped with bismuth oxide, Radiat. Phys. Chem. (2023), 110875, https://doi.org/10.1016/j.radphyschem.2023.110875.

[20] R. Rajaramakrishna, W. Chaiphaksa, Garima Garima, K.N. Sharvani, S. Kothan, Jakrapong Kaewkhao, Phys. Status Solidi 220 (10) (2023), 2200411, https://doi.org/10.1002/pssa.202370020.

[21] M. Mahmoud, S.A. Makhlouf, B. Alshahrani, et al., Silicon 14 (2022) 2905–2919, https://doi.org/10.1007/s12633-021-01062-y.

[22] Y. Al-Hadeethi, M.I. Sayyed, J. Kaewkhao, Bahaaudin M. Raffah, Rahma Almalki, R. Rajaramakrishna, An extensive investigation of physical, optical and radiation shielding properties for borate glasses modified with gadolinium oxide, Appl. Phys. A 125 (749) (2019) 1–10.

[23] Y. Al-Hadeethi, M.I. Sayyed, J. Kaewkhao, A. Askin, Bahaaudin M. Raffah, E.M. Mkawi, R. Rajaramakrishna, Physical, structural, optical, and radiation shielding properties of B2O3–Gd2O3–Y2O3 glass system, Appl. Phys. A 125 (852) (2019) 1–7.

[24] Kh S. Shaaban, B.M. Alotaibi, El Sayed Yousef, J. Electron. Mater. 52 (2023) 3591–3603, https://doi.org/10.1007/s11664-023-10347-4.

[25] Haifa A. Alyousef, Z.A. Alrowaili, Mohamed Saad, Hussain Al-Mohiy, A. Abdulaziz, Alshihri, S. Kh, Shaaban, M.S. Al-Buriahi, E.A. Abdel Wahab, Heliyon 9 (3) (2023), e14435, https://doi.org/10.1016/j.heliyon.2023.e14435.

[26] Y.S. Rammah, F.I. El-Agawany, E.A. Abdel Wahab, M.M. Hessien, KhS. Shaaban, Radiat. Phys. Chem. 193 (2022), 109956, https://doi.org/10.1016/j. radphyschem.2021.109956.
[27] W.M. Haynes, David R. Lide, Thomas J. Bruno, CRC Handbook of Chemistry and Physics, 93rd edition, CRC press, 2012-13, pp. 9–21.
[28] C.G. Liu, J. Zhang, L.J. Chen, J. Wen, L.Y. Dong, D.Y. Yang, Y.H. Li, Int. J. Mod. Phys. B 31 (2017), 1750184, https://doi.org/10.1142/S0217979217501843.
[29] R. Rajaramakrishna, Y. Ruangtaweepa, S. Sattayaporn, P. Kidkhunthod, S. Kothan, J. Kaewkhao, Radiat. Phys. Chem. 171 (2020), 108695, https://doi.org/ 10.1016/j.radphyschem.2020.108695.
[30] J. Tauc, Optical properties and electronic structure of amorphous Ge and Si, Mater. Res. Bull. 3 (1968) 37–46, https://doi.org/10.1016/0025-5408(68)90023-8.
[31] Ashok Bhogi, Boora Srinivas, Papolu Padmavathi, Kasarapu Venkataramana, Kiran Kumar Ganta, Mohd Shareefuddin, Puram Kistaiah, Opt. Mater. 133 (2022), 112911, https://doi.org/10.1016/j.optmat.2022.112911.
[32] N. Ghobadi, Band gap determination using absorption spectrum fitting procedure, Int. Nano Lett. 3 (2013) 2, https://doi.org/10.1186/2228-5326-3-2.
[33] M.S. Al-Buriahi, Canel Eke, Z.A. Alrowaili, Ateyyah M. Al-Baradi, B.T. Imen Kebaili, Tonguc, Optik 249 (2022), 168257, https://doi.org/10.1016/j. ijleo.2021.168257.
[34] Amani Alalawi, M.S. Al-Buriahi, M.I. Sayyed, H. Akyildirim, H. Arslan, M.H.M. Zaid, B.T. Tonguc, Ceram. Int. 46 (11) (2020) 17300–17306, https://doi.org/ 10.1016/j.ceramint.2020.04.017.
[35] M.S. Al-Buriahi, D.K. Gaikwad, H.H. Hegazy, et al., J. Mater. Sci. Mater. Electron. 32 (2021) 9440–9451, https://doi.org/10.1007/s10854-021-05608-z.
[36] M.S. Al-Buriahi, I.O. Olarinoye, Sultan Alomairy, Imen Kebaili, Rumeysa Kaya, Halil Arslan, Baris T. Tonguc, Prog. Nucl. Energy 137 (2021), 103763, https:// doi.org/10.1016/j.pnucene.2021.103763.
[37] P. Limkitjaroenporn, J. Kaewkhao, P. Limsuwan, W. Chewpraditkul, J. Phys. Chem. Solid. 72 (Issue 4) (2011) 245–251, https://doi.org/10.1016/j. jpcs.2011.01.007.
[38] G. Sathiyapriya, K.A. Naseer, K. Marimuthu, E. Kavaz, A. Alalawi, M.S. Al-Buriah, J. Mater. Sci. Mater. Electron. 32 (2021) 8570–8592, https://doi.org/ 10.1007/s10854-021-05499-0.
[39] S. Manohara, S. Hanagodimath, L. Gerward, Radiat. Phys. Chem. 79 (5) (2010) 575.
[40] mp-1204405: Bi2O3 (Cubic, Ia-3, 206) (materialsproject.org).
[41] mp-504886: Gd2O3 (Cubic, Ia-3, 206) (materialsproject.org).
[42] S. Raut, V. Awasarmol, S. Shaikh, B. Ghule, S. Ekar, R. Mane, P. Pawar, Radiat. Eff. Defect Solid 173 (3–4) (2018) 329.
[43] S. Kh, a Shaaban, M. Ateyyah, b Al-Baradi, B.M. Alotaibi c, A.F. Abd El-Rehim, J. Mater. Res. Technol. 23 (2023) 756–764.
[44] Y.S. Rammah, F.I. El-Agawany, E.A. Abdel Wahab, M.M. Hessien, KhS. Shaaban, Radiat. Phys. Chem. 193 (2022), 109956, https://doi.org/10.1016/j. radphyschem.2021.109956.
[45] E.A.A. Wahab, E.M. Ahmed, Y.S. Rammah, et al., J. Inorg. Organomet. Polym. 32 (2022) 3983–3996, https://doi.org/10.1007/s10904-022-02400-2.
[46] I.I. Bashter, Calculation of radiation attenuation coefficients for shielding concretes, Ann. Nucl. Energy 24 (1997) 1389–1401.
[47] Kh S. Shaaban, Ateyyah M. Al-Baradi, Atif Mossad Ali, RSC Adv. 12 (2022) 3036–3043, https://doi.org/10.1039/d2ra00171c.
[48] A. Angnanon, S. Nualpralaksana, B. Damdee, R. Rajaramakrishna, N. Chanlek, M. Horprathum, S. Kothan, Kaewkhao, Radiation Physics and Chemistry 201 (2022), 110406, https://doi.org/10.1016/j.radphyschem.2022.110406.
[49] B. Damdee, K. Kirdsiri, H.J. Kim, K. Yamanoi, N. Wongdamnern, P. Kidkhunthod, R. Rajaramakrishna, J. Kaewkhao, Radia. Chem. Phys 200 (2022), 110386, https://doi.org/10.1016/j.radphyschem.2022.110386.
[50] R. Rajaramakrishna, P. Nijapai, P. Kidkhunthod, H.J. Kim, J. Kaewkhao, J. Alloys Compd. 813 (2020), 151914.
[51] N. Wantana, E. Kaewnuam, Y. Ruangtaweep, D. Valiev, S. Stepanov, K. Yamanoi, H.J. Kim, J. Kaewkhao, Radiat. Phys. Chem. 164 (2019), 108350.